Journal of Biomedical Optics

SPIEDigitalLibrary.org/jbo

Noninvasive Raman spectroscopy of rat tibiae: approach to *in vivo* assessment of bone quality

Paul I. Okagbare
Dana Begun
Mary Tecklenburg
Ayorinde Awonusi
Steven A. Goldstein
Michael D. Morris

SPIE

Noninvasive Raman spectroscopy of rat tibiae: approach to *in vivo* assessment of bone quality

Paul I. Okagbare,[a] Dana Begun,[b] Mary Tecklenburg,[c] Ayorinde Awonusi,[c] Steven A. Goldstein,[b] and Michael D. Morris[a]
[a]University of Michigan, Department of Chemistry, Ann Arbor, Michigan
[b]University of Michigan, Medical School, Orthopedic Research Laboratories, Department of Orthopedic Surgery, Ann Arbor, Michigan
[c]Central Michigan University, Department of Chemistry, Mt. Pleasant, Michigan

Abstract. We report on *in vivo* noninvasive Raman spectroscopy of rat tibiae using robust fiber-optic Raman probes and holders designed for transcutaneous Raman measurements in small animals. The configuration allows placement of multiple fibers around a rat leg, maintaining contact with the skin. Bone Raman data are presented for three regions of the rat tibia diaphysis with different thicknesses of overlying soft tissue. The ability to perform *in vivo* noninvasive Raman measurement and evaluation of subtle changes in bone composition is demonstrated with rat leg phantoms in which the tibia has carbonated hydroxylapatite, with different carbonate contents. Our data provide proof of the principle that small changes in bone composition can be monitored through soft tissue at anatomical sites of interest in biomedical studies. [DOI: 10.1117/1.JBO.17.9.090502]

Keywords: carbonated hydroxyapatite; fiber-optic probes; in-vivo Raman; rat tibia.

Paper 12343L received Jun. 11, 2012; revised manuscript received Jul. 29, 2012; accepted for publication Jul. 31, 2012; published online Sep. 6, 2012.

1 Introduction

Bone undergoes continuous remodeling in response to loading, local damage, and pathologies. Remodeling of bone changes its chemical composition, which is an important indicator of its physiological status and mechanical competence.[1,2] The ability to measure changes in chemical composition of bone is, therefore, important.[2–4] Existing noninvasive technologies used to monitor bone evaluate the morphology and calcium content, but provide no direct information on other properties of the tissue.[5–9] Vibrational spectroscopy has proved useful in the study of bone development, bone biomechanics, and bone pathologies because it provides this composition information.[10,11] Unlike infrared spectroscopy, which provides essentially similar information, Raman spectroscopy suffers little from water interference; therefore, it is applicable to fresh tissue and *in vivo* measurements.[12]

Address all correspondence to: Michael D. Morris, University of Michigan, Department of Chemistry, Ann Arbor, Michigan. Tel: 734-769-3758; Fax: 734-615-3796; E-mail: mdmorris@umich.edu

However, *in vivo* Raman spectroscopy has its own challenges, including background fluorescence from tissue components (especially skin melanin), interfering protein spectral bands from overlying soft tissue, and the multiple scattering that is characteristic of almost all tissues.[13] These challenges limit the depth from which Raman signals can be collected.

Realizing the potential for *in vivo* studies requires fiber-optic probes that are configured for transcutaneous Raman measurement on a time scale ranging from a few seconds to one or 2 min. Our laboratory has developed several fiber-optic probes based on spatial separation of excitation and collection fibers that allow bone Raman spectroscopy through layers of overlying tissue.[14,15] The principle is well known in tissue spectroscopy; in the literature, it is called spatially offset Raman spectroscopy.[16,17] A limitation of spatial offsetting is that measurement time increases rapidly as the depth of penetration increases. We have previously demonstrated backscattering in *in vivo* collection of murine Raman spectra at depths of a few millimeters in mice[18] and low-definition Raman tomography in excised tissue at thicknesses of more than 2 cm.[19] These measurements have required unrealistically long times. Here, we describe and test a probe configuration adapted from diffuse optical tomography that reduces measurement time to 60 s at several positions along a rat tibia.

We have previously reported cadaveric rat tibia studies using a diffuse tomography-based probe containing 50 collection fibers terminated in stainless steel ferrules and a single excitation fiber that could be positioned at one of several points around the tibia.[20] The fibers were mounted in a conformal silicone holder.

In the present design, the fifty 100-μm silica core fibers are grouped into 10 bundles of five fibers each, providing greater mechanical robustness. A single 300-μm silica core excitation fiber is used. A demountable aluminum fiber holder that can be positioned reproducibly around the leg of the rat replaces the silicone holder used previously (Fig. 1).[20] The fiber holder is constructed as two pieces to facilitate rapid placement and removal. O-rings mounted through holes arranged around the circumference of the holder allow the easy insertion and removal of fibers. The design allows a sequence of measurements with the excitation fiber placed at a different position in each measurement to optimize the collection of bone spectra. The aluminum holder is easily positioned at different points along the tibial diaphysis. The placement of the illumination and collection probes generates adequate spatial offset for transcutaneous Raman measurement on rat limbs. The collection fibers are arranged into a linear array for coupling to the input slit of a Raman spectrograph. The Raman instrument is an axial transmissive Raman spectrograph equipped with an 830-nm excitation laser and a 256 × 1024 front-illuminated CCD for collection of near-infrared light (RamanRxn1, Kaiser Optical Systems Inc., Ann Arbor, MI).

Using this probe and a holder with single-fiber illumination, bone Raman spectra were acquired for 60 s at three regions along the diaphysis of the tibia of an anesthetized rat, as shown in Fig. 1(c). This sequence allowed measurement through different thicknesses of overlying soft tissue. The acquired Raman data were processed in MATLAB (MathWorks, Inc., Natick, MA) as previously described to remove cosmic ray spikes, grating-induced curvature, and grating/detector

0091-3286/2012/$25.00 © 2012 SPIE

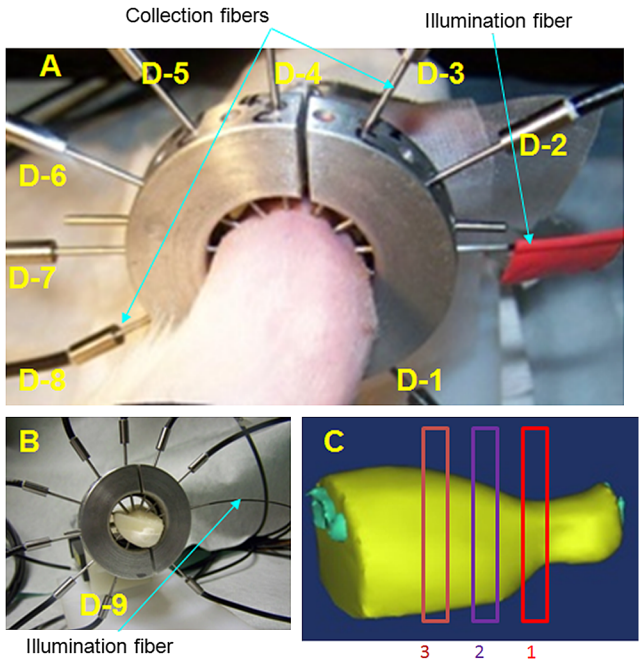

Fig. 1 Noninvasive Raman spectroscopy of a rat tibia. (a) The probe holder is fastened to a bed on which the rat lies while anesthetized. The fibers (D1–D9) are adjustable, as shown with a phantom. (b) The phantom mimics the anatomy and spectroscopy of rat leg. (c) A rat leg rendering showing the three regions along the diaphysis where Raman spectra were obtained.

misalignment.[20,21] The spectra are reported as wavenumber shifts and are corrected for detector quantum efficiency variation after background subtraction (tissue autofluorescence removal).[20,22] Figure 2(a) presents unsmoothed Raman spectra from the three diaphysial positions without any removal of overlying tissue contributions. As expected, the intensity of the bone mineral band at 960 cm^{-1} relative to collagen protein bands at 1450 and 1660 cm^{-1} is greater for region 1 (960/1660 = 3.06), where the maximum thickness of the overlying soft tissue is about 1 mm. There are increasing contributions from the overlying tissue signal in regions 2 and 3 [~0.5 cm (960/1, 660 = 1.94) and ~1 cm (960/1660 = 1.57) maximum thickness, respectively]. In every case, one or more detectors (fibers) views bone underneath a thin layer of tissue due to the anatomy of the rat leg, so mineral/collagen intensities do not scale linearly with the maximum soft tissue thickness. For example, in region 3, detector fiber 1 is located over the tibia with ~5 mm of soft tissue thickness from the underlying bone, while detectors 2, 3, 4, and 5, and 6, 7, 8, and 9 are more than ~8.5 mm and ~14.1 mm, respectively, from the underlying bone. In region 2, fiber 1 is positioned at ~3 mm, fibers 2, 3, 4, and 5 at ~4.6 mm and fibers 6, 7, 8, and 9 at ~7 mm from the bone. In region 1, all fibers are positioned with approximately the same soft tissue separation (~1 mm) from the underlying bone. The variation in acquired bone mineral Raman signal intensities relative to each individual fiber position is shown in Fig. 2(b) for region 2.

Overlying tissue contributions cause changes in the relative intensities of the protein bands with respect to the mineral band. To separate the bone Raman spectrum from soft tissue contribution, band target entropy minimization (BTEM)[23] was performed on the spectra from the three regions using the first few eigenvectors of the singular value decomposition (SVD) matrix.[18] The unsmoothed recovered spectra for the three regions are shown in Fig. 2(c). Soft tissue contributions to the spectra are minimized, but not completely removed, after BTEM and the intensities of the bone mineral band at 960 cm^{-1} relative to collagen protein bands are enhanced in regions 2 and 3. The incomplete removal of soft tissue by BTEM could be associated with the short acquisition time, the signal-to-noise ratio, and the limited number of input spectra into the BTEM algorithm. These results suggest that this probe configuration is suitable for longitudinal spectroscopic studies of fracture healing, among other subjects. The probe can be positioned in 1-min measurements made in 1 min, and the probe removed in a few seconds. *in vivo* Raman spectroscopy can consume a small fraction of the 30-min maximum duration of anesthesia.

Carbonate substitution is one of the proposed Raman metrics for evaluating bone quality.[3] Because of the proximity of $CO_3^{-2}\nu_1$ to a component of $PO_4^{-3}\nu_3$ it is notoriously difficult to measure band intensity accurately.[24] We demonstrated the ability to measure small changes in bone compositions using multilayer phantoms that model geometric, optical, and spectroscopic rat leg properties.[20,25] The phantoms were constructed with carbonated hydroxyapatite containing different amounts of carbonate as the bone mineral model.[20,25] Raman spectra

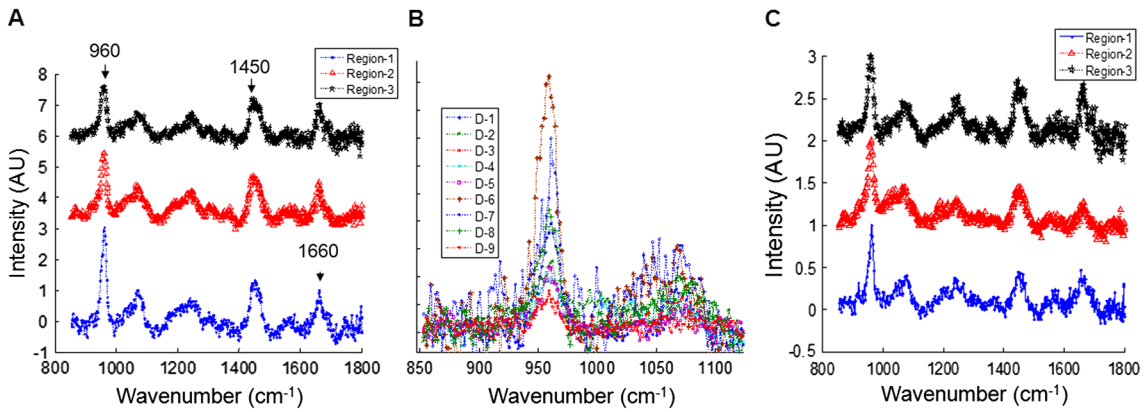

Fig. 2 Raman spectra from three different regions of rat leg along the tibial diaphysis. Spectra were normalized to the protein band at 1660 cm^{-1}. (b) Raman spectra from the individual fibers labeled D1–D9 in the wavelength range of 850 to 1100 cm^{-1}. The intensities of the phosphate (bone mineral) band varied with fiber positions. (c) Recovered bone Raman spectra after BTEM was performed on the data in (a) for the three regions. Soft tissue contributions are minimized to recover the bone Raman spectrum. Spectra were normalized to the mineral band at 960 cm^{-1}.

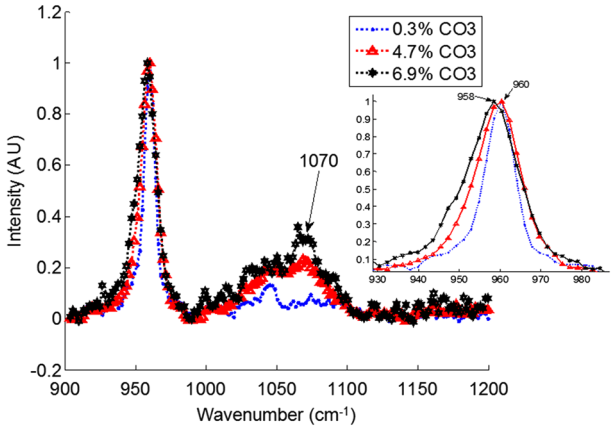

Fig. 3 Transcutaneous Raman spectra acquired from rat leg. The rat leg models were constructed using carbonated hydroxyapatite with varied level of carbonate substitution (0.3%, 4.7%, and 6.9% carbonated hydroxyapatite) as the tibia model. Differences between specimens were captured in the Raman spectra. Intensity of the carbonate band at 1070 cm^{-1} and the width of the phosphate band at 960 cm^{-1} both increase with carbonate substitution. The expanded view of the spectra in (a) showing the wavenumber range from 930 to 980 cm^{-1} is presented as an insert. The position of the $PO_4^{-3}\nu_1$ peak shifted from 960 to 958 cm^{-1} with increasing carbonate substitution.

of the phantoms were acquired at the laser powers and measurement times used for the rat tibia. The resulting Raman spectra are shown in Fig. 3. The band intensities at 1070 cm^{-1} for the 0.3%, 4.7% and 6.9% CO_3^{-2} values increase with increasing carbonate substitution. The width of $PO_4^{-3}\nu_1$ at ~960 cm also increases with increasing carbonate substitution and shifts to lower wavenumber (see Fig. 3 insert), as reported for the salts.[24] The full-width half-maximum of the $PO_4^{-3}\nu_1$ band scales linearly ($r^2 = 0.99$) with CO_3^{-2} content (the linear plot is not shown in Fig. 3). These data provide proof of the principle that small changes in bone composition can be monitored through at least a 1-cm layer of soft tissue.

Our results complement the results of our previous report on the distal tibiae of mice, which have a thinner layer of soft tissue.[18] Although we have not directly addressed noninvasive human subject bone spectroscopy, our results suggest that at some sites, 1-min measurements are feasible.

Acknowledgments

The authors acknowledge support of this work through National Institutes of Health (NIH) Grants R01AR055222 and R01AR056646. The authors also thank Kathleen Sweet for help with animal handling and Charles Roehm for construction of the optical fiber holder.

References

1. X. Feng and J. M. McDonald, "Disorders of Bone Remodeling," *Annual Review of Pathology: Mechanisms of Disease*, Vol. 6, A. K. Abbas, S. J. Galli, and P. M. Howley, Eds., *Ann. Rev.*, 121–145, Palo Alto (2011).
2. S. Gamsjäger et al., "Raman application in bone imaging," in *Raman Spectroscopy for Soft Matter Applications*, pp. 225–267, John Wiley & Sons, Inc., Hoboken, New Jersey (2009).
3. M. Morris, "Raman spectroscopy of bone and cartilage," in *Emerging Raman Applications and Techniques in Biomedical and Pharmaceutical Fields*, P. Matousek and M. D. Morris, Eds., pp. 347–364, Springer, Berlin Heidelberg (2010).
4. J. R. Maher et al., "Raman spectroscopy detects deterioration in biomechanical properties of bone in a glucocorticoid-treated mouse model of rheumatoid arthritis," *J. Biomed. Opt.* **16**(8), 087012 (2011).
5. M. L. Brandi, "Micro architecture, the key to bone quality," *Rheum.* **48**, IV3–IV8 (2009).
6. O. D. Kennedy and F. J. O'Brien, *Bone Quality: Where Should We Be Looking?* Nova Science Publishers, Inc., Hauppauge, NY (2009).
7. H. K. Genant, K. Engelke, and S. Prevrhal, "Advanced CT bone imaging in osteoporosis," *Rheumatology* **47**, 9–16 (2008).
8. T. M. Link, "Osteoporosis imaging: state of the art and advanced imaging," *Radiology* **263**(1), 3–17 (2012).
9. T. Vokes and M. Favus, "Noninvasive assessment of bone structure," *Curr. Osteo. Rep.* **1**(1), 20–24 (2003).
10. E. Donnelly, "Methods for assessing bone quality: a review," *Clin. Orthop. Rel. Res.* **469**(8), 2128–2138 (2011).
11. A. L. Boskey and R. Mendelsohn, "Infrared spectroscopic characterization of mineralized tissues," *Vib. Spectrosc.* **38**(1–2), 107–114 (2005).
12. M. D. Morris and G. S. Mandair, "Raman assessment of bone quality," *Clin. Orthop. Rel. Res.* **469**(8), 2160–2169 (2011).
13. M. V. Schulmerich et al., "Optical clearing in transcutaneous Raman spectroscopy of murine cortical bone tissue," *J. Biomed. Opt.* **13**(2), 021108 (2008).
14. M. V. Schulmerich et al., "Transcutaneous fiber optic Raman spectroscopy of bone using annular illumination and a circular array of collection fibers," *J. Biomed. Opt.* **11**(6), 060502 (2006).
15. M. V. Schulmerich et al., "Subsurface and transcutaneous Raman spectroscopy and mapping using concentric illumination rings and collection with a circular fiber-optic array," *Appl. Spectrosc.* **61**(7), 671–678 (2007).
16. P. Matousek et al., "Subsurface probing in diffusely scattering media using spatially offset Raman spectroscopy," *Appl. Spectrosc.* **59**(4), 393–400 (2005).
17. P. Matousek, "Inverse spatially offset Raman spectroscopy for deep noninvasive probing of turbid media," *Appl. Spectrosc.* **60**(11), 1341–1347 (2006).
18. M. V. Schulmerich et al., "Transcutaneous Raman spectroscopy of murine bone *in vivo*," *Appl. Spectrosc.* **63**(3), 286–295 (2009).
19. M. V. Schulmerich et al., "Noninvasive Raman tomographic imaging of canine bone tissue," *J. Biomed. Opt.* **13**(2), 020506 (2008).
20. P. I. Okagbare et al., "Development of non-invasive Raman spectroscopy for *in vivo* evaluation of bone graft osseointegration in a rat model," *Analyst* **135**(12), 3142–3146 (2010).
21. F. W. Esmonde-White, K. A. Esmonde-White, and M. D. Morris, "Minor distortions with major consequences: correcting distortions in imaging spectrographs," *Appl. Spectrosc.* **65**(1), 85–98 (2011).
22. C. A. Lieber and A. Mahadevan-Jansen, "Automated method for subtraction of fluorescence from biological Raman spectra," *Appl. Spectrosc.* **57**(11), 1363–1367 (2003).
23. E. Widjaja et al., "Band-target entropy minimization (BTEM) applied to hyperspectral Raman image data," *Appl. Spectrosc.* **57**(11), 1353–1362 (2003).
24. A. Awonusi, M. D. Morris, and M. M. J. Tecklenburg, "Carbonate assignment and calibration in the raman spectrum of apatite," *Calcif. Tissue Int.* **81**(1), 46–52 (2007).
25. F. W. L. Esmonde-White et al., "Biomedical tissue phantoms with controlled geometric and optical properties for Raman spectroscopy and tomography," *Analyst* **136**(21), 4437–4446 (2011).